ACS APPLIED MATERIALS & INTERFACES

Research Article

www.acsami.org

Ordered-Mesoporous-Carbon-Bonded Cobalt Phthalocyanine: A Bioinspired Catalytic System for Controllable Hydrogen Peroxide Activation

Nan Li,[†] Wangyang Lu,*[,†] Kemei Pei,[‡] Yuyuan Yao,[†] and Wenxing Chen*[,†]

[†]National Engineering Lab for Textile Fiber Materials & Processing Technology (Zhejiang), Zhejiang Sci-Tech University, Hangzhou 310018, China

[‡]Department of Chemistry, Zhejiang Sci-Tech University, Hangzhou 310018, China

Supporting Information

ABSTRACT: The chemistry of enzymes presents a key to understanding the catalysis in the world. In the pursuit of controllable catalytic oxidation, researchers make extensive efforts to discover and develop functional materials that exhibit various properties intrinsic to enzymes. Here we describe a bioinspired catalytic system using ordered-mesoporous-carbon (OMC)-bonded cobalt tetraaminophthalocyanine (CoTAPc-OMC) as a catalyst that could mimic the space environment and reactive processes of metalloporphyrin-based heme enzymes and employing linear dodecylbenzenesulfonate as the fifth ligands to control the activation of H_2O_2 toward the peroxidase-like oxidation. The generation of nonselective free hydroxyl radicals was obviously inhibited. In addition, functional modification of OMC has been achieved by a moderate method, which can reduce excessive damage to the structure of OMC. Because of its favorable and tunable pore texture, CoTAPc-OMC provides a suitable interface and environment for the accessibility and oxidation of C.I. Acid Red 1, the model compound, and exhibits significantly enhanced catalytic activity and sufficient stability for H_2O_2 activation. The high-valent cobalt oxo intermediates with high oxidizing ability have been predicted as the acceptable active species, which have been corroborated by the results from the semiempirical quantum-chemical PM6 calculations.

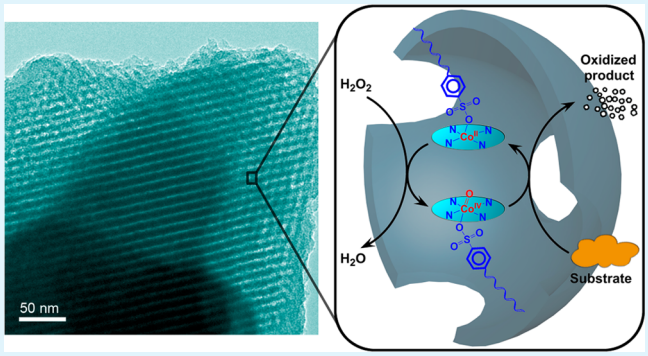

KEYWORDS: *ordered mesoporous carbon, cobalt phthalocyanine, bioinspired catalysis, hydrogen peroxide activation*

INTRODUCTION

Oxidation reactions using hydrogen peroxide (H_2O_2) as an oxidant are fundamentally important to industrial synthetic chemistry, biomimetic chemistry, and environmental chemistry.[1−3] As an environmentally friendly reagent, H_2O_2 does not give rise to any waste products and fulfills the requirement of green chemistry.[4] However, one disadvantage of H_2O_2 is that it can undergo radical-induced decomposition to H_2O and $^1/_2O_2$. Therefore, the activation of H_2O_2 to oxidize the substrates corresponding to enzymatic peroxidase-catalyzed reactions is desired for the majority of oxidations. Typically, during the activation of H_2O_2 catalyzed by transition-metal complex catalysts, homolytic cleavage and heterolytic cleavage of the peroxide O−O bond are in competition, leading to the production of hydroxyl radicals ($^{\bullet}$OH) and metal-based oxidants, respectively.[5] For oxidation reactions that employ coordination complexes as catalysts, $^{\bullet}$OH is recognized to be a poor selectivity species that can move freely to touch and oxidize any organic matter in aqueous solution and even autodecompose the complex catalysts.[6] Hence, the controllable activation of H_2O_2 is important for catalytic systems with a coordination complex to minimize the generation of unselective $^{\bullet}$OH, meaning that a more selective metal-based oxidant should be obtained by promoting heterolytic cleavage of the O−O bond. The catalytic processes of peroxide-activated enzymes such as peroxidase can provide a source of inspiration for us, in which the spatial environment and the fifth ligands are the two key factors to control the reaction channels.[7−9] Our main interest here is to construct a bioinspired catalytic system with environment and reaction channel-like enzymes by employing metallophthalocyanines (MPcs) as the catalytic entity, which are typical coordination complexes like metalloporphyrins (MPs) and have been widely used in many catalytic reactions because of their convenient synthesis and good stability.[5] Many transition-metal catalysts have been designed and synthesized to mimic the reaction of enzymes;[10−12] however, they do not present the features of enzymes such as selectivity and steric accessibility, which are mainly determined by the natural

Received: February 5, 2014
Accepted: March 27, 2014
Published: March 27, 2014

environment of enzymes.[13] For the design of an enzyme-mimic system, the closer analogies of the enzyme should require a suitable cavity or cleft for accessibility of the substrates and the introduction of functional groups that act as binding sites, coenzyme analogues, or catalytic sites within the cavity.[14,15] One must admit that the protein structure of enzymes is difficult to imitate and protein is easily damaged. Thus, finding materials that have stable structure and suitable pore sizes to construct a three-dimensional (3D) environment is more conducive to facilitating the peroxidase-like oxidation.

Owing to the remarkable properties including high surface area, uniform pore size, and tunable pore texture, ordered mesoporous carbon (OMC) shows advantages in energy storage, energy conversion, catalysis, and adsorption of bulky molecules.[16,17] The porous interface structures of OMC materials allow them to have great potential for improving the reaction solution immersion and providing an effective space for substrate diffusion.[17−19] With its continuously expanded 3D structure and relatively larger pore size, OMC is promising as a carrier of enzymes for the conversion of larger molecular substrates and the reduction of mass-transfer limitation.[20] Moreover, our previous studies found that carbon nanotubes (CNTs) with a special sp^2-hybridized surface and excellent electrical properties could dramatically improve the activity of cobalt phthalocyanine (CoPc) for H_2O_2 activation,[21,22] and activated carbon fiber (ACF) could enhance the catalytic performance of CoPc for the oxidation of phenols in the presence of H_2O_2,[23] but it seemed useless for larger substrate molecules such as dye molecules because of the microporous structure (pore size < 2 nm) of the ACF. Given its larger and tunable pore texture, OMC is more appropriate for the catalytic oxidation of larger substrates as a highly promising candidate of the backbone surrounding the catalytic entity like the protein structure in enzymes.

Herein, we report a bioinspired catalytic system based on OMC-bonded cobalt tetraaminophthalocyanine (CoTAPc-OMC), which imitates the peroxidase enzymes from their structure and reactive process for controllable H_2O_2 activation, including the catalytic entity of cobalt tetraaminophthalocyanine (CoTAPc) and the backbone of OMC surrounding the CoTAPc centers, and brings linear dodecylbenzenesulfonate (LAS, which is widely used in household detergents as well as in numerous industrial applications, thus causing LAS to be widespread in most industrial and domestic wastewater) as the fifth ligand to bear on the channels of H_2O_2 activation. A relatively mild method has been conducted to functionally modify the OMC. Control of the reaction channels for H_2O_2 activation has been investigated, and enhanced catalytic activity has been evidenced by the oxidation experiments of the model compound, C.I. Acid Red 1 (AR1; Scheme S1 in the Supporting Information, SI). We reveal the mechanism of CoTAPc-OMC activating H_2O_2 and explore the effect of the pore structure and LAS ligands on the reaction channels. The semiempirical quantum-chemical PM6 method has been performed to support inference on the mechanisms of CoTAPc-OMC activating H_2O_2 with and without LAS.

EXPERIMENTAL SECTION

Catalyst Preparation. CoTAPc and OMC were synthesized according to the description in refs 24 and 25. OMC (0.1 g) was dispersed in 400 mL of ultrapure water. After 4.5 g of potassium persulfate (KPS) was added and the pH value was adjusted to 12, the reaction solution was stirred and kept at 85 °C for 3 h. The cooled reaction solution was centrifuged and washed with ultrapure water until the filtrate was neutral; carboxyl-containing OMC was obtained after drying under vacuum. Carboxyl-containing OMC (0.1 g) and CoTAPc (0.005 g) were ultrasonically dispersed in dimethyl sulfoxide, *N*,*N*′-dimethylpyridin-4-amine and *N*,*N*′-dicyclohexylcarbodiimide were added, and the reaction was stirred at room temperature for 24 h. The product was filtered and washed with *N*,*N*′-dimethylformamide several times to remove ungrafted CoTAPc. The final product was washed with methylene chloride, ultrapure water, and ethanol. CoTAPc-OMC was obtained after drying (Scheme S2 in the SI).

H_2O_2 Activation Experiment. The activity of CoTAPc-OMC activating H_2O_2 in aqueous solution was investigated by the oxidation of AR1, whose concentration is proportional to its absorbance in the UV−vis spectrum. The catalytic oxidation of AR1 (50 μM) was carried out in the presence of CoTAPc-OMC (0.2 g L^{-1}) at a constant temperature of 50 °C and pH 10 with or without the addition of LAS (2.5 mM) as the fifth ligand. The oxidation was initiated when H_2O_2 (10 mM) was added into the solution. Continuous cycle experiments were performed 11 times. For every run, a known concentration of the AR1 was added into the reaction system to maintain the initial concentration of 50 μM, and an equal volume of H_2O_2 (one third of the initial H_2O_2 concentration in the first cycle) was added per cycle starting from the next cycle. The reaction solution had been adjusted to the desired pH value by $HClO_4$ and NaOH.

Equipment. X-ray photoelectron spectroscopy (XPS) was employed to investigate the chemical bonding of carboxyl-containing OMC and CoTAPc-OMC on a Thermo Scientific K-Alpha spectrometer (monochromatic Al Kα, 1486.6 eV). In addition, the chemical structures of CoTAPc, OMC, carboxyl-containing OMC, and CoTAPc-OMC were analyzed with Fourier transform infrared (FTIR) spectra (Thermo Nicolet 5700). The UV−vis absorption spectra were obtained on a Hitachi U-3010 spectrophotometer. The Brunauer−Emmett−Teller (BET) surface areas and pore volumes were determined by N_2 adsorption on a Micromeritics ASAP 2020 sorptometer at 77 K. The transmission electron microscopy (TEM) image was acquired on a JEOL JEM-2010 microscope. The morphology of OMC, carboxyl-containing OMC, and CoTAPc-OMC was observed by field-emission scanning electron microscopy (FESEM; ZEISS ULTRA 55). The thermal stability was investigated with a Mettler Toledo TGA/DSC 1 using under a nitrogen atmosphere at a flow rate of 50 mL min^{-1}, with a heating rate of 20 °C min^{-1}. The cobalt content in CoTAPc-OMC was measured using microwave-assisted digestion−flame atomic absorption spectrometry, allowing calculation of the content of CoTAPc in CoTAPc-OMC as 29.6 μmol g^{-1}, and about 5−6 CoTAPc units were anchored within every pore of OMC by approximate calculation. The electron paramagnetic resonance (EPR) signals were detected on a Bruker A300 spectrometer at room temperature with settings as follows: center field, 3517.5 G; sweep width, 80 G; microwave frequency, 9.88 GHz; modulation frequency, 100 kHz; power, 20 mW. 5,5-Dimethyl-1-pyrroline *N*-oxide (DMPO) was used as the spin trapper for the probable radicals.

RESULTS AND DISCUSSION

XPS data show the chemical bonding in OMC, carboxyl-containing OMC, and CoTAPc-OMC. The XPS spectra from a wide scan (Figure 1a) showed that the oxygen content increased significantly after being oxidized (compared with OMC), indicating a large number of oxygen-containing groups existed on carboxyl-containing OMC. The immobilization of CoTAPc on OMC can also be preliminarily proposed by the new peaks of cobalt and nitrogen in the XPS spectrum of CoTAPc-OMC. In order to investigate the bonding modes, the high-resolution spectra of O 1s, C 1s, N 1s, and Co 2p were deconvoluted into single peaks. Figure 1b shows the C 1s spectrum of carboxyl-containing OMC; the main peak at 284.48 eV is assigned to C−C 1s, and the other peaks are assigned to −C−OH (286.28 eV), −C═O (287.78 eV), and

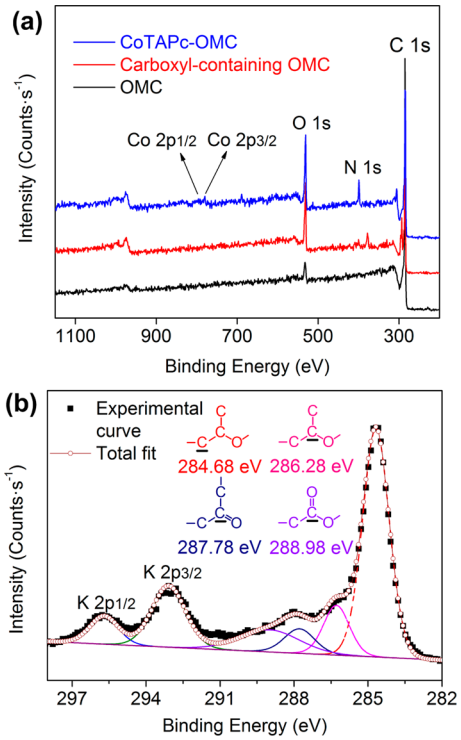

Figure 1. (a) XPS spectra of OMC, carboxyl-containing OMC, and CoTAPc-OMC (the spectral region was 250−1150 eV). (b) XPS C 1s spectra of carboxyl-containing OMC.

−COO− (288.98 eV), suggesting that carboxyl-containing OMC was obtained by KPS oxidizing OMC.[26] Here, the presence of −COOK can be evidenced by the addition of HCl into the solution with carboxyl-containing OMC, where obvious flocculation was observed when the pH value was below 3. Moreover, it can be seen from the O 1s peaks in Figure S1 in the SI that untreated OMC contains a small amount of oxygen, which is attributed to the low concentration of defects,[27] and the increased oxygen contents in carboxyl-containing OMC observed at 530.94 and 533.28 eV are assigned to C═O and C−O−H.[22] When CoTAPc was immobilized on OMC, the portion of the C−O−H peak (533.25 eV) was much smaller than that of C═O (531.18 eV), indicating that part of C−O−H was consumed by the amidation reaction. Further, the N 1s and Co 1s peaks give coincident information about the more detailed bonding environment of CoTAPc-OMC. In Figure S2 in the SI, we can observe that the N 1s peaks occurring at 398.65 and 399.89 eV are attributed to aza bridging, pyrrole nitrogen atoms, and the external amino substituent of CoTAPc.[22] The peak at 400.82 eV (Figure S2c in the SI) may be explained by the nitrogen atom of the amide group (−NH−CO−) being used for bonding between the carboxyl and substituted amino groups. Also, similar results can be seen in their XPS Co 2p spectra (Figure S3 in the SI). In addition, the weak absorption peak at 550−750 nm in the UV−vis spectra of CoTAPc-OMC (Figure S4 in the SI) and the slight absorption peak at 1000−1200 cm^{-1} in the FTIR spectrum (Figure S5 in the SI) can also confirm that CoTAPc was immobilized on OMC.

To understand the morphologies of the as-prepared OMC and CoTAPc-OMC, their FESEM images are shown in Figure S6 in the SI. No obvious difference in the surface morphology can be observed. The pore structure of OMC, carboxyl-containing OMC, and CoTAPc-OMC were investigated using TEM and N_2 adsorption. TEM images of OMC, carboxyl-containing OMC, and CoTAPc-OMC displayed a well-ordered mesoporous arrangement with the uniform size, and OMC showed an almost imperceptible collapse or destruction region after being oxidized by KPS (Figure 2). Corresponding to the results from Figure 3, they exhibited the typical type IV isotherm with hysteresis loops and a capillary condensation step in partial pressures of 0.45−0.8, indicating that the mesopore size was all quite uniform. It also can be confirmed that OMC, carboxyl-containing OMC, and CoTAPc-OMC have a narrow pore-size distribution in the mesopore range with a size of around 6 nm. According to the calculated results from N_2 adsorption−desorption isotherms, the BET surface area of OMC is 636 $m^2\ g^{-1}$ with a pore volume of 0.499 $cm^3\ g^{-1}$, which decreased to 337 $m^2\ g^{-1}$ and 0.354 $cm^3\ g^{-1}$ after being oxidized; this might be explained by the fact that oxygen-containing groups on the walls lead to a decrease in the pore volume.[28] Here, OMC was partially oxidized to form carboxyl-containing OMC, which can also be confirmed by their FTIR spectra. The weak peak of C═O at around 1720 cm^{-1} (Figure S5 in the SI) has indeed been found. The TEM image of CoTAPc-OMC displayed no obvious difference from those of OMC and carboxyl-containing OMC (Figure 2), the surface area and pore volume are 407 $m^2\ g^{-1}$ and 0.357 $cm^3\ g^{-1}$, and the anchor of CoTAPc showed minor effects on the pore size, pore volume, and surface area, indicating that the method for functional modification of OMC was moderate enough that almost no

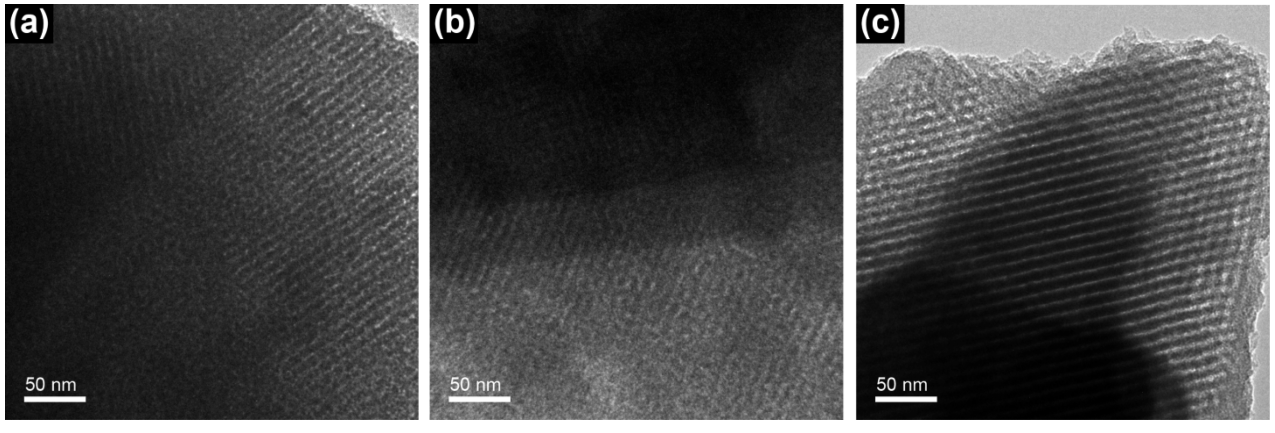

Figure 2. TEM images of (a) OMC, (b) carboxyl-containing OMC, and (c) CoTAPc-OMC.

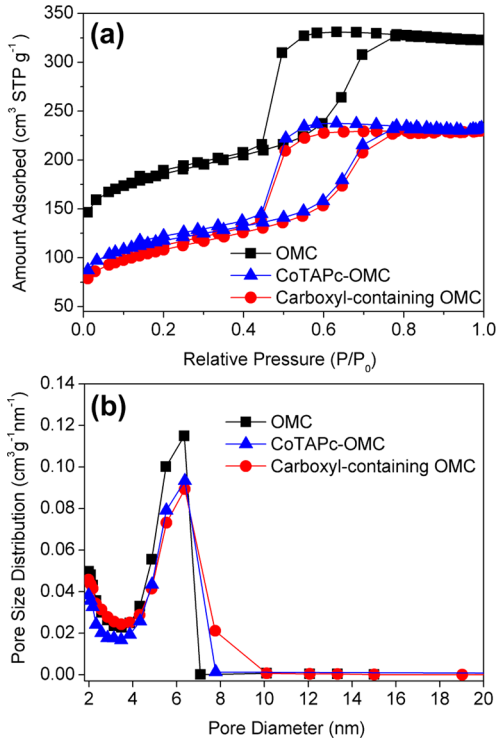

Figure 3. (a) N_2 adsorption−desorption isotherms at 77 K. (b) Corresponding pore-size distribution curves, estimated from the adsorption branch of N_2 isotherms by the Barrett−Joyner−Halenda method.

obvious destruction region was introduced to the structure of OMC. Moreover, results of the thermal stability test are shown in Figure S7 in the SI. It can be seen that OMC has excellent thermal stability in the range 50−800 °C, and it significantly reduced after being oxidized because of the increased carboxyl group. The thermal stability of CoTAPc-OMC is between those of CoTAPc and carboxyl-containing OMC, presenting a similar curve with carboxyl-containing OMC; this might be caused by the unreacted carboxyl groups and the covalently bonded CoTAPc with higher stability.

The catalytic activity of the bioinspired system based on CoTAPc-OMC has been conducted using AR1 as the model. As shown in Figure 4, almost no catalytic activity has been exhibited by LAS in the absence of CoTAPc-OMC, as well as other systems with CoTAPc or OMC (Figure S8 in the SI), and

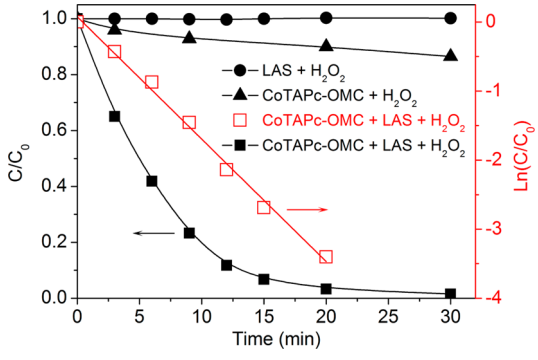

Figure 4. Concentration changes of AR1 (5×10^{-5} M) under different conditions ([CoTAPc-OMC] = 0.2 g L^{-1} (containing 5.9 μM CoTAPc), [LAS] = 2.5 mM, [H_2O_2] = 0.01 M, pH 10, 50 °C).

weak catalytic activity has been presented in the system containing CoTAPc-OMC and H_2O_2. However, in the presence of CoTAPc-OMC, LAS, and H_2O_2, AR1 could be oxidized quickly, and the reaction follows first-order kinetics. Comparative experiments showed that LAS could give a slight enhancement for CoTAPc-OMC adsorbing AR1 without H_2O_2 (Figure 5) and the adsorption of AR1 reached equilibrium

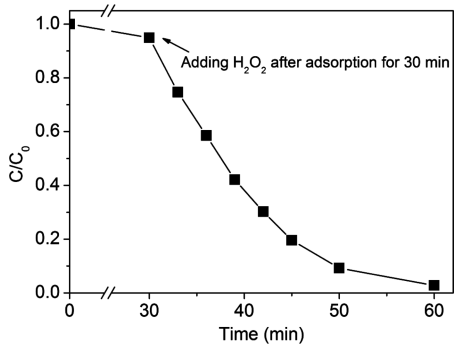

Figure 5. Concentration changes of AR1 (5×10^{-5} M) by the addition of H_2O_2 after adsorption for 30 min ([CoTAPc-OMC] = 0.2 g L^{-1}, [LAS] = 2.5 mM, [H_2O_2] = 0.01 M, pH 10, 50 °C).

within a short time. However, the concentration of AR1 declined rapidly once H_2O_2 was added to the system, indicating that LAS not only acts as a surfactant to promote the adsorption of AR1 into CoTAPc-OMC but induces a crucial effect on the reaction channel to achieve high catalytic efficiency for AR1 oxidation by CoTAPc-OMC activating H_2O_2.

In our previous studies, the activity for activating H_2O_2 was enhanced by introducing CNTs as the support, but the high activity for substrate oxidation had been achieved at a higher H_2O_2 concentration because the reaction of H_2O_2 was so fast that most of H_2O_2 had been consumed by the generation of H_2O and O_2.[22] We have been trying to find a viable way to control the reaction channel of H_2O_2 activation to avoid the catalase-like process, for example, to control oxidation toward the peroxidase-like process by means of an interface reaction,[23] but the catalase-like activity had not been inhibited because of the unchanged reactive pathway. Interestingly, nearly no O_2 evolution has been observed and utilization of H_2O_2 has been greatly improved in this catalytic system containing LAS, implying that the reaction channels might be changed by the introduction of LAS. Moreover, the compared experiments were carried out in the presence of ACF-supported CoTAPc (CoTAPc-ACF), which was prepared according to our previous report[23] and had microporous structure. The results showed that there was no obvious oxidation of the model compound AR1 in the CoTAPc-ACF/H_2O_2 system with or without LAS (Figure S8 in the SI). However, in the CoTAPc-OMC/H_2O_2 system, the rapid oxidation of AR1 can be achieved in the presence of LAS. Because OMC has a continuously expanded 3D structure and a relatively larger pore texture, which is important for the conversion of larger molecular substrates and reduces mass-transfer limitation. Therefore, OMC played an important role in speeding up the reaction by promoting dye diffusion into the active sites.

Additionally, the relatively large pore size of OMC allows the AR1 molecules to approach the active sites and be oxidized; thus, the Lineweaver−Burk plot of the peroxidase-like activity of CoTAPc-OMC with LAS has been obtained and shown in

Figure 6 to provide evidence for the peroxidase-like activity. The inverse of the initial reaction rate and substrate

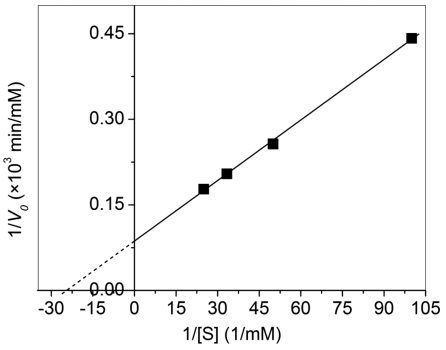

Figure 6. Lineweaver–Burke plot for the peroxidase-like activity of CoTAPc-OMC activating H_2O_2 with AR1 as the substrate.

concentration increases linearly, indicating that the binding probability between active sites and substrates is increasing as the substrate concentration increases, and H_2O_2 activation catalyzed by CoTAPc-OMC with LAS exhibits the typical characters corresponding to the enzymatic reaction, which cannot be presented by the catalytic reaction based on $^{\bullet}OH$ species. Also, the kinetic constants are represented in Table 1 according to the Michaelis–Menten mode.

Table 1. Kinetic Constants of CoTAPc-OMC Activating H_2O_2

K_m (mM)	V_{max} (μM s^{-1})	k_{cat} (s^{-1})	k_{cat}/K_m (s^{-1} mM^{-1})
0.041	0.195	0.033	0.804

Generally, the supported MPcs lose partial activity because the barriers consisted of reaction intermediates, which would prevent the substrates from approaching the active sites after a long reaction time, finally resulting in the loss of activity. For some peroxide-activating catalysts of metal complexes, a primary importance is to avoid autocatalytic decomposition of these complexes, which inevitably occurs during catalytic oxidation dominated by highly reactive and nonselective $^{\bullet}OH$, especially in aqueous solution. Thus, the stability of the catalysts is very important for complex catalysts. Here the repetitive cyclic oxidation of AR1 has been sustained 11 times in this catalytic system involving CoTAPc-OMC, LAS, and H_2O_2. It can be seen from the results in Figure 7 that this catalytic system exhibited high peroxidase-like activity for activating H_2O_2 to oxidize AR1 in each successive cycle, indicating that CoTAPc-OMC has a strong influence on the activity and stability. It is noteworthy that high activity has been achieved by this catalytic system even without supplementary LAS during cyclic oxidation because LAS might be adsorbed into CoTAPc-OMC and coordinated with the cobalt ions and a balance was maintained until the end of the reaction.

On the basis of the results above, LAS is absolutely critical for H_2O_2 activation catalyzed by CoTAPc-OMC. To the best of our knowledge, hydroxyl radical oxidation[29,30] and nonradical oxidation (e.g., high-valent iron–oxo species)[31,32] seem to dominate the catalytic mechanisms of MPs/MPcs activating H_2O_2 and other peroxides. Compared to the poor selective $^{\bullet}OH$ species, the metal–oxo species have a high oxidative capacity for substrates with significant chemoselectivity,

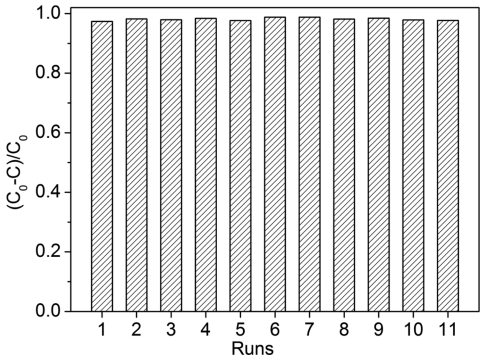

Figure 7. Cyclic catalytic oxidation of AR1 (5×10^{-5} M). Each cycle typically lasts 20 min ([CoTAPc-OMC] = 0.2 g L^{-1}, [LAS] = 2.5 mM, [H_2O_2] = 0.01 M, pH 10, 50 °C).

regioselectivity, stereoselectivity and/or enantioselectivity.[33] Thus, how to minimize the generation of $^{\bullet}OH$ is the key to a good catalytic system when the catalytic entity is a coordination complex. As shown in Figure 8, no DMPO–$^{\bullet}OH$

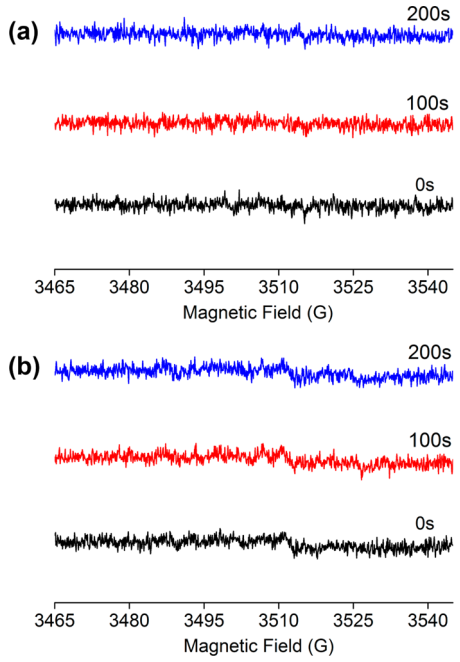

Figure 8. DMPO spin-trapping EPR spectra in aqueous (a) and ethanol (b) solution containing AR1 (5×10^{-5} M; [CoTAPc-OMC] = 0.2 g L^{-1}, [LAS] = 2.5 mM, [H_2O_2] = 0.01 M, [DMPO] = 0.02 M).

and DMPO–$^{\bullet}OOH$ signals have been observed in aqueous or ethanol solution with LAS, suggesting that this system performs a nonradical process. However, in a typical Fenton system (Fe^{2+}/H_2O_2), an obvious DMPO–$^{\bullet}OH$ signal has been observed in aqueous solution (Figure S9 in the SI). Considering the lower dosage (one tenth) of H_2O_2 by comparison with a CoTAPc–CNTs system,[21] together with the EPR results, a different nonradical reaction channel has indeed been performed by the introduction of LAS.

In the reactions of the two major classes of peroxide-activating enzymes, peroxidases can activate H_2O_2 to oxidize substrates and catalases promote the decomposition of H_2O_2 into O_2 and H_2O.[10] Moreover, the fifth ligand could have a great contribution to the reaction channels in MP-based

enzymatic reactions;[34−36] for instance, horseradish peroxidase presents peroxidase-like activity by the presence of the imidazole ligand of histidine residue, while catalase presents catalase-like activity by the presence of the phenolate ligand of tyrosine residue.[7,9] It can be confirmed that the desired reactive intermediates are accessible by using the proper fifth ligands, meaning that cleavage of the O−O bond could be controlled by coordination of the fifth ligands.

As poor ligands, the SO_3^- group of aryl sulfonates always gives a weaker coordination ability with many transition-metal (such as Co^{2+}, Cu^{2+}, Ni^{2+}, etc.) complexes than that of water molecules in aqueous solution.[37−40] However, the O atom from SO_3^- will coordinate with the divalent metal ions when these divalent metals lie on an inversion center and are coordinated by N atoms.[41−44] In CoTAPc-OMC, there are two positions axial to the ligands: one site is coordinated with the O atom from SO_3^- of aryl sulfonates, and the other site can be reserved for H_2O_2. It has been reported that the fifth ligands with electron donor capability could provide a "push" effect and help heterolytically cleave the O−O bond of H_2O_2, leading to reactive intermediates.[45] We can confirm that the addition of LAS, which acts as the fifth ligands to H_2O_2 activation, induces heterolytic cleavage of the O−O bond and results in a different nonradical reaction channel. The mechanism has also been studied using the semiempirical quantum-chemical PM6 method by modeling the graphite as a coronene-like planar sheet due to the graphite crystals of OMC (see the model in Scheme S3 in the SI).[46] It can be seen from Table S1 in the SI that the Co−O bond distance (1.678 Å) is shorter than that of Co−O (SO_3^-) (1.937 Å) in the presence of LAS, thereby facilitating heterolysis of the O−O bond. Furthermore, without LAS, the frontier orbitals with relatively lower energy such as SOMO−2, SOMO−3, and SOMO−4 orbitals (SOMO = singly occupied molecular orbital) in the system with CoTAPc-OMC and H_2O_2 are clearly localized on the C atoms of the graphite planar sheet ($S = {}^5/_2$; Figure 9a). Thus, the unpaired electrons on the C atoms of OMC could attach H_2O_2 and lead to inefficient oxidation of the substrate (Figure 4) due to H_2O_2 decomposition into O_2 and H_2O, corresponding to the inference in the previous study.[23] As a comparison, SOMO−1 and SOMO−2 with a lower energy in the system with CoTAPc-OMC, LAS, and H_2O_2 are located principally nearby the Co ions ($S = {}^3/_2$; Figure 9b), suggesting that the matched frontier orbitals on cobalt−oxo could participate in the substrate oxidation.

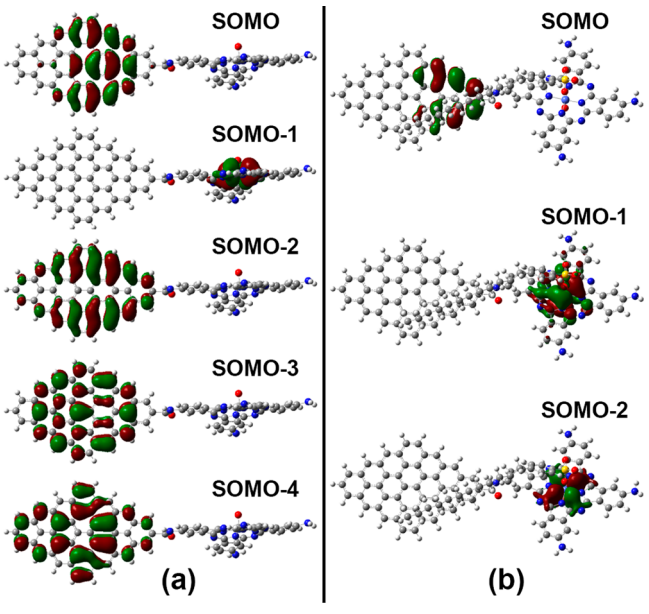

Figure 9. Presentation of frontier orbitals for the energy-minimized PM6 models of the formed cobalt−oxo intermediates in CoTAPc-OMC without (a) or with (b) LAS.

Further, the nonhydroxyl radical oxidations catalyzed by MPs and cytochrome P450 have been extensively studied, and their active oxidizing species, high-valent transition metal−oxo intermediates were identified and characterized.[11,47−49] The high oxidation states of the central transition-metal ions are more inclined to be stabilized in MPs, while the phthalocyanine ligand tends to stabilize the lower oxidation states of metal compared to that of porphyrin, implying that the high oxidation states of MPcs should have stronger oxidizing ability than those of MPs.[50] Sorokin and co-workers have focused on the generation and characterization of high-valent iron−oxo phthalocyanines, which were generally accepted to be the key reactive intermediates in some oxidations catalyzed by iron phthalocyanine with H_2O_2 or other peroxides.[11,31,51,52] Therefore, we believe that high-valent cobalt−oxo species have been formed during H_2O_2 activation catalyzed by CoTAPc-OMC in the presence of LAS, together with the spatial structure constructed by OMC for accessibility of the substrates, and the high peroxidase-like activity has been achieved.

CONCLUSIONS

We have developed a bioinspired catalytic system based on CoTAPc-OMC activating H_2O_2, in which CoTAPc acts as the catalytic entity and OMC with a relatively large pore texture gives a feasible environment for the accessibility of relatively larger substrates to the active sites. A high peroxidase-like activity has been achieved and the reaction channel of H_2O_2 activation has been controlled by the introduction of LAS, which acts as the fifth ligand and helps cleave the O−O bond of H_2O_2 heterolytically, inhibiting the production of $^{\bullet}OH$. We inferred that the high-valent cobalt−oxo intermediates are the possible active species in this peroxidase-like system. This inference has been also corroborated by the results of PM6 calculations. Moreover, this catalytic system is stable for reuse and resistant to autodecomposition of the catalytic entity. This study attempts to construct an enzyme−mimic system by applying OMC as a backbone to support the catalytic entity, and the introduction of the fifth ligands mimics the functions of cofactors in a natural enzyme, providing a source of inspiration to design catalysts of artificial enzymes for practical applications. Furthermore, this study can offer a facile but highly effective approach to improving the overall catalytic performance of traditional catalysts and realizing catalytic reactions that were not possible in the past.

ASSOCIATED CONTENT

Supporting Information

Synthesis of CoTAPc-OMC, XPS O 1s, N 1s, and Co 2p data, molecular structure and concentration changes of AR1, dynamic thermogravinmetric analytical results, FESEM images, FTIR and UV−vis spectra, and calculated bond lengths for the energy-minimized PM6 models. This material is available free of charge via the Internet at http://pubs.acs.org.

AUTHOR INFORMATION

Corresponding Authors

*E-mail: luwy@zstu.edu.cn.
*E-mail: wxchen@zstu.edu.cn.

Author Contributions

The manuscript was written through contributions of all authors. All authors have given approval to the final version of the manuscript.

Notes

The authors declare no competing financial interest.

ACKNOWLEDGMENTS

This work was supported by the National Natural Science Foundation of China (Grants 51133006 and 51103133), Zhejiang Provincial Natural Science Foundation of China (Grants Y14E030044 and Y14E030049) and Textile Vision Science & Education Fund.

REFERENCES

(1) Brégeault, J. M. Transition-Metal Complexes for Liquid-Phase Catalytic Oxidation: Some Aspects of Industrial Reactions and of Emerging Technologies. *Dalton Trans.* **2003**, 3289−3302.

(2) Mahammed, A.; Gross, Z. Albumin-Conjugated Corrole Metal Complexes: Extremely Simple Yet Very Efficient Biomimetic Oxidation Systems. *J. Am. Chem. Soc.* **2005**, *127*, 2883−2887.

(3) Sharma, R. K.; Gulati, S.; Pandey, A.; Adholeya, A. Novel, Efficient and Recyclable Silica Based Organic−Inorganic Hybrid Nickel Catalyst for Degradation of Dye Pollutants in a Newly Designed Chemical Reactor. *Appl. Catal., B* **2012**, *125*, 247−258.

(4) Piera, J.; Bäckvall, J. E. Catalytic Oxidation of Organic Substrates by Molecular Oxygen and Hydrogen Peroxide by Multistep Electron Transfer—A Biomimetic Approach. *Angew. Chem., Int. Ed.* **2008**, *47*, 3506−3523.

(5) Sorokin, A. B. Phthalocyanine Metal Complexes in Catalysis. *Chem. Rev.* **2013**, *113*, 8152−8191.

(6) Collins, T. J. TAML Oxidant Activators: A New Approach to the Activation of Hydrogen Peroxide for Environmentally Significant Problems. *Acc. Chem. Res.* **2002**, *35*, 782−790.

(7) Berglund, G. I.; Carlsson, G. H.; Smith, A. T.; Szöke, H.; Henriksen, A.; Hajdu, J. The Catalytic Pathway of Horseradish Peroxidase at High Resolution. *Nature* **2002**, *417*, 463−468.

(8) Filizola, M.; Loew, G. H. Role of Protein Environment in Horseradish Peroxidase Compound I Formation: Molecular Dynamics Simulations of Horseradish Peroxidase−HOOH Complex. *J. Am. Chem. Soc.* **2000**, *122*, 18−25.

(9) Reid, T. J., III; Murthy, M. R.; Sicignano, A.; Tanaka, N.; Musick, W. D.; Rossmann, M. G. Structure and Heme Environment of Beef Liver Catalase at 2.5 Å Resolution. *Proc. Natl. Acad. Sci. U.S.A.* **1981**, *78*, 4767−4771.

(10) Ghosh, A.; Mitchell, D. A.; Chanda, A.; Ryabov, A. D.; Popescu, D. L.; Upham, E. C.; Collins, G. J.; Collins, T. J. Catalase-Peroxidase Activity of Iron(III)-TAML Activators of Hydrogen Peroxide. *J. Am. Chem. Soc.* **2008**, *130*, 15116−15126.

(11) Zhang, R.; Horner, J. H.; Newcomb, M. Laser Flash Photolysis Generation and Kinetic Studies of Porphyrin−Manganese−Oxo Intermediates. Rate Constants for Oxidations Effected by Porphyrin−Mn^{V}−Oxo Species and Apparent Disproportionation Equilibrium Constants for Porphyrin−Mn^{IV}−Oxo Species. *J. Am. Chem. Soc.* **2005**, *127*, 6573−6582.

(12) Zhang, Z.; Hao, J.; Yang, W.; Lu, B.; Ke, X.; Zhang, B.; Tang, J. Porous Co_3O_4 Nanorods−Reduced Graphene Oxide with Intrinsic Peroxidase-Like Activity and Catalysis in the Degradation of Methylene Blue. *ACS Appl. Mater. Interfaces* **2013**, *5*, 3809−3815.

(13) Ball, Z. T. Designing Enzyme-like Catalysts: A Rhodium(II) Metallopeptide Case Study. *Acc. Chem. Res.* **2013**, *46*, 560−570.

(14) Kuwabara, J.; Stern, C. L.; Mirkin, C. A. A Coordination Chemistry Approach to a Multieffector Enzyme Mimic. *J. Am. Chem. Soc.* **2007**, *129*, 10074−10075.

(15) Wulff, G. Enzyme-like Catalysis by Molecularly Imprinted Polymers. *Chem. Rev.* **2002**, *102*, 1−28.

(16) Zhuang, X.; Wan, Y.; Feng, C.; Shen, Y.; Zhao, D. Highly Efficient Adsorption of Bulky Dye Molecules in Wastewater on Ordered Mesoporous Carbons. *Chem. Mater.* **2009**, *21*, 706−716.

(17) Liang, C.; Li, Z.; Dai, S. Mesoporous Carbon Materials: Synthesis and Modification. *Angew. Chem., Int. Ed.* **2008**, *47*, 3696−3717.

(18) Park, J. B.; Lee, J.; Yoon, C. S.; Sun, Y. K. Ordered Mesoporous Carbon Electrodes for Li−O_2 Batteries. *ACS Appl. Mater. Interfaces* **2013**, *5*, 13426−13431.

(19) Zeng, L.; Zheng, C.; Deng, C.; Ding, X.; Wei, M. MoO_2-Ordered Mesoporous Carbon Nanocomposite as an Anode Material for Lithium-Ion Batteries. *ACS Appl. Mater. Interfaces* **2013**, *5*, 2182−2187.

(20) Zhou, Z.; Hartmann, M. Progress in Enzyme Immobilization in Ordered Mesoporous Materials and Related Applications. *Chem. Soc. Rev.* **2013**, *42*, 3894−3912.

(21) Lu, W.; Li, N.; Chen, W.; Yao, Y. The Role of Multiwalled Carbon Nanotubes in Enhancing the Catalytic Activity of Cobalt Tetraaminophthalocyanine for Oxidation of Conjugated Dyes. *Carbon* **2009**, *47*, 3337−3345.

(22) Lu, W.; Li, N.; Bao, S.; Chen, W.; Yao, Y. The Coupling of Metallophthalocyanine with Carbon Nanotubes to Produce a Nanomaterial-Based Catalyst for Reaction-Controlled Interfacial Catalysis. *Carbon* **2011**, *49*, 1699−1709.

(23) Lu, W.; Chen, W.; Li, N.; Xu, M.; Yao, Y. Oxidative Removal of 4-Nitrophenol Using Activated Carbon Fiber and Hydrogen Peroxide to Enhance Reactivity of Metallophthalocyanine. *Appl. Catal., B* **2009**, *87*, 146−151.

(24) Chen, W.; Lu, W.; Yao, Y.; Xu, M. Highly Efficient Decomposition of Organic Dyes by Aqueous-Fiber Phase Transfer and in Situ Catalytic Oxidation Using Fiber-Supported Cobalt Phthalocyanine. *Environ. Sci. Technol.* **2007**, *41*, 6240−6245.

(25) Wang, X.; Liang, C.; Dai, S. Facile Synthesis of Ordered Mesoporous Carbons with High Thermal Stability by Self-Assembly of Resorcinol−Formaldehyde and Block Copolymers under Highly Acidic Conditions. *Langmuir* **2008**, *24*, 7500−7505.

(26) El-Merraoui, M.; Tamai, H.; Yasuda, H.; Kanata, T.; Mondori, J.; Nadai, K.; Kaneko, K. Pore Structures of Activated Carbon Fibers from Organometallics/Pitch Composites by Nitrogen Adsorption. *Carbon* **1998**, *36*, 1769−1776.

(27) Darmstadt, H.; Roy, C.; Kaliaguine, S.; Choi, S. J.; Ryoo, R. Surface Chemistry of Ordered Mesoporous Carbons. *Carbon* **2002**, *40*, 2673−2683.

(28) Bazuła, P. A.; Lu, A. H.; Nitz, J. J.; Schüth, F. Surface and Pore Structure Modification of Ordered Mesoporous Carbons via a Chemical Oxidation Approach. *Microporous Mesoporous Mater.* **2008**, *108*, 266−275.

(29) Tao, X.; Ma, W.; Zhang, T.; Zhao, J. Efficient Photooxidative Degradation of Organic Compounds in the Presence of Iron Tetrasulfophthalocyanine under Visible Light Irradiation. *Angew. Chem., Int. Ed.* **2001**, *40*, 3014−3016.

(30) Chen, S. L.; Huang, X. J.; Xu, Z. K. Effect of a Spacer on Phthalocyanine Functionalized Cellulose Nanofiber Mats for Decolorizing Reactive Dye Wastewater. *Cellulose* **2012**, *19*, 1351−1359.

(31) Afanasiev, P.; Kudrik, E. V.; Albrieux, F.; Briois, V.; Koifman, O. I.; Sorokin, A. B. Generation and Characterization of High-Valent Iron Oxo Phthalocyanines. *Chem. Commun.* **2012**, *48*, 6088−6090.

(32) Kudrik, E. V.; Afanasiev, P.; Alvarez, L. X.; Du-bourdeaux, P.; Clémancey, M.; Latour, J.; Blondin, G.; Bouchu, D.; Albrieux, F.; Nefedov, S. E.; Sorokin, A. B. An N-Bridged High-Valent Diiron−Oxo Species on a Porphyrin Platform That Can Oxidize Methane. *Nat. Chem.* **2012**, *4*, 1024−1029.

(33) Que, L.; Tolman, W. B. Biologically Inspired Oxidation Catalysis. *Nature* **2008**, *455*, 333−340.

(34) Collman, J. P.; Sorrell, T. N.; Dawson, J. H.; Trudell, J. R.; Bunnenberg, E.; Djerassi, C. Magnetic Circular Dichroism of Ferrous Carbonyl Adducts of Cytochromes P-450 and P-420 and Their Synthetic Models: Further Evidence for Mercaptide as the Fifth Ligand to Iron. *Proc. Natl. Acad. Sci. U.S.A.* **1976**, *73*, 6−10.
(35) Werck-Reichhart, D.; Feyereisen, R. Cytochromes P450: A Success Story. *Genome Biol.* **2000**, *1*, 3003.1−3003.9.
(36) Thomas, C. M.; Ward, T. R. Artificial Metalloenzymes: Proteins as Hosts for Enantioselective Catalysis. *Chem. Soc. Rev.* **2005**, *34*, 337−346.
(37) Du, J.; Li, Q.; Li, W.; Lin, H.; Guo, G. Hexaaquacobalt(II) 4-Hydroxybenzenesulfonate Dehydrate. *Acta Crystallogr., Sect. E: Struct. Rep. Online* **2007**, *E63*, m2597−m2597.
(38) Couldwell, C.; Prout, K.; Robey, D.; Taylor, R. The Crystal and Molecular Structures of Hexaaquacopper(II) Benzenesulphonate, Toluene-4-sulphonate and D-Camphor-10-sulphonate. *Acta Crystallogr., Sect. B: Struct. Crystallogr. Cryst. Chem.* **1978**, *B34*, 1491−1499.
(39) Kosnic, E. J.; McClymont, E. L.; Hodder, R. A.; Squattrito, P. J. Synthesis and Structures of Layered Metal Sulfonate Salts. *Inorg. Chim. Acta* **1992**, *201*, 143−151.
(40) Cai, J.; Chen, C.; Liao, C.; Feng, X.; Chen, X. Solid-State Structures of Group 1 and Group 2 Metal 1,5-Naphthalenedisulfonates: Systematic Investigation of Lamellar Three-Dimensional Networks Constructed by Metal Arenedisulfonate. *Acta Crystallogr., Sect. B: Struct. Sci.* **2001**, *B57*, 520−530.
(41) Zhang, K.; Meng, X.; Li, X. Bis(4-aminobenzenesulfonato-κO)bis-(propane-1,3-diamine-κ^2 N,N′)copper(II) Dehydrate. *Acta Crystallogr., Sect. E: Struct. Rep. Online* **2009**, *E65*, m1678−m1679.
(42) Murase, I.; Vuckovic, G.; Kodera, M.; Harada, H.; Matsumoto, N.; Kida, S. Synthesis and Characterization of Copper(II), Nickel(II), and Cobalt(II) Binuclear Complexes with a New Tricyclic Octadentate Ligand, 1,5,8,12,15,19,22,26-Octaazatricyclo-[17.9.2.25,15]dotriacontane (tcoa): Trapping of Carbon Dioxide in a Neutral Aqueous Solution. *Inorg. Chem.* **1991**, *30*, 728−733.
(43) Sundberg, M. R.; Sillanpääb, R. Syn versus Anti Conformation in Monodentately Coordinated Sulfonate Groups. Crystal Structure Determination and MMX Force-Field Calculations for *trans*-Di(4-methylbenzenesulfonato)bis(1,3-diaminopropane)copper(II), $C_{20}H_{34}CuN_4O_6S_2$. *Acta Chem. Scand.* **1993**, *47*, 1173−1178.
(44) Cocker, T. M.; Bachman, R. E. Isolation and Crystal Structure of a Novel Dinuclear Nickel(II) O-bound Sulfinate from the Oxidation of 2,2′-Bipyridine-1,2-benzenedithiolatonickel(II). *Chem. Commun.* **1999**, 875−876.
(45) Sono, M.; Roach, M. P.; Coulter, E. D.; Dawson, J. H. Heme-Containing Oxygenases. *Chem. Rev.* **1996**, *96*, 2841−2888.
(46) Gupta, G.; Slanac, D. A.; Kumar, P.; Wiggins-Camacho, J. D.; Wang, X.; Swinnea, S.; More, K. L.; Dai, S.; Stevenson, K. J.; Johnston, K. P. Highly Stable and Active Pt−Cu Oxygen Reduction Electrocatalysts Based on Mesoporous Graphitic Carbon Supports. *Chem. Mater.* **2009**, *21*, 4515−4526.
(47) Pan, Z.; Wang, Q.; Sheng, X.; Horner, J. H.; Newcomb, M. Highly Reactive Porphyrin−Iron−Oxo Derivatives Produced by Photolyses of Metastable Porphyrin−Iron(IV) Diperchlorates. *J. Am. Chem. Soc.* **2009**, *131*, 2621−2628.
(48) Rittle, J.; Green, M. T. Cytochrome P450 Compound I: Capture, Characterization, and C−H Bond Activation Kinetics. *Science* **2010**, *330*, 933−937.
(49) Sorokin, A. B.; Tuel, A. Metallophthalocyanine Functionalized Silicas: Catalysts for the Selective Oxidation of Aromatic Compounds. *Catal. Today* **2000**, *57*, 45−59.
(50) Afanasiev, P.; Kudrik, E. V.; Millet, J. J. M.; Bouchu, D.; Sorokin, A. B. High-Valent Diiron Species Generated from N-bridged Diiron Phthalocyanine and H_2O_2. *Dalton Trans.* **2011**, *40*, 701−710.
(51) Zalomaeva, O. V.; Ivanchikova, I. D.; Kholdeeva, O. A.; Sorokin, A. B. Kinetics and Mechanism of the Oxidation of Alkyl Substituted Phenols and Naphthols with ^{t}BuOOH in the Presence of Supported Iron Phthalocyanine. *New J. Chem.* **2009**, *33*, 1031−1037.
(52) Afanasiev, P.; Bouchu, D.; Kudrik, E. V.; Millet, J. J. M.; Sorokin, A. B. Stable N-Bridged Diiron(IV) Phthalocyanine Cation Radical Complexes: Synthesis and Properties. *Dalton Trans.* **2009**, 9828−9836.